RSC Advances

PAPER

View Article Online
View Journal | View Issue

Cite this: *RSC Adv.*, 2021, **11**, 37067

Experimental study on light volatile products from thermal decomposition of lignin monomer model compounds: effect of temperature, residence time and methoxyl group†

Huamei Yang, * Ju Jiang, Bingzhe Zhang and Panpan Xu

Received 8th September 2021
Accepted 22nd October 2021

DOI: 10.1039/d1ra06743e

rsc.li/rsc-advances

In order to investigate the effects of temperature, residence time (RT) and methoxyl (OCH_3) on the product distribution and vapor phase reactions during pyrolysis of complex solid fuels, three model phenolic representatives, phenol, guaiacol and syringol, were pyrolyzed at a residence time of 0.7 s, over a temperature range of 400 °C–950 °C, and at temperatures of 650 °C and 750 °C, in a RT region of 0.1 s–4.2 s. Increasing yields of CO and C_1–C_5 light hydrocarbons (LHs) with RT at 650 °C and 750 °C indicated that ring-reduction/CO elimination of phenolic compounds happened at 650 °C, and dramatically at 750 °C. The addition of OCH_3 affects the product distribution and ring-reduction pathways: C_5 LHs from phenol, C_2 LHs, C_4 LHs and C_5 LHs from guaiacol, and C_1–C_2 LHs from syringol. CO_2 yields increase with the addition of OCH_3. CO_2 was formed *via* benzoyl and a four-membered ring, which would compete with the CO formation. The addition of OCH_3 promotes the formation of coke and tar. The decomposition pathways are discussed, based on the experimental data, focusing on ring-reduction reactions and the formation of CO/CO_2 and C_1–C_5 LHs.

1. Introduction

Solid carbon resources such as coal and biomass can be converted to afford carbon-based chemicals and materials, fuels, and electrical power by thermochemical conversion processes, such as liquefaction, pyrolysis, gasification, and combustion.[1–6] Pyrolysis has attracted much attention in the past decades due to its feasibility and huge commercial outlook.[2,5] At the same time, pyrolysis is also the initial step of gasification.[3] Hence, it is significant to elucidate the typical pyrolysis mechanism of carbon resources. Pyrolysis was always described as two conversion stages: primary pyrolysis from solid fuels to volatiles, and vapor-phase reactions of volatiles generated from primary pyrolysis.[6–9] Vapor-phase reactions are inevitable and key steps for the formation of final products during the pyrolysis of solid carbon resources.[8,9]

Aromatic structures are rich in solid carbon resources, and how the aromatic structure reacts during pyrolysis has aroused wide concerns.[7–14] Model compounds were employed to investigate the detailed reaction pathways involved in pyrolysis mechanism of coal and biomass. Dimmer or oligomer of lignin units were widely employed to experimentally or numerically investigate the breakage of ether bonds or carbon–carbon linkages among aromatic structures in lignin.[14–19] Cleavage mechanisms of β-O-4 linkage and α-O-4 linkage are the main topics, and were analyzed with free-radical reactions, molecular rearrangements, and concerted elimination reactions.[15–17]

Recently, monomer model compounds were decomposed, and it was reported that inorganic gases (IGs) and light hydrocarbons (LHs) were dominant products generated from pyrolysis of monomer aromatic model compounds through ring-reduction reactions at 650–850 °C.[11,20–38] Considering the ring-reductions reactions of aromatic structure to small fragments, the decomposition mechanisms of monomer phenolic compounds such as phenol,[21,22] catechol,[23–26] anisole,[27–29] guaiacol,[7,30–34] syringol,[34–36] eugenol[37] and vanillin[38] have recently been investigated experimentally and theoretically.

Guaiacyl, syringyl, and *p*-hydroxylphenyl structures are rich in volatiles generated from pyrolysis of solid carbon resources, especially from pyrolysis of lignin.[1,39] Understanding the conversion mechanism of guaiacyl, syringyl, and *p*-hydroxylphenyl structures is of great importance for improvement of thermochemical conversion processes during pyrolysis of solid carbon resources, especially a study of the gas-phase chemistry. Phenol as the simplest model compounds of *p*-hydroxylphenyl structures has been widely investigated, and the main pathway of phenol decomposition was to form CO and cyclopentadiene by the ring-reduction as Path 1.[21,22]

School of Materials and Chemical Engineering, Xuzhou University of Technology, Xuzhou, Jiangsu 221018, China. E-mail: yhmcumt@yeah.net

† Electronic supplementary information (ESI) available: Chromatographic conditions and compounds detected were listed. See DOI: 10.1039/d1ra06743e

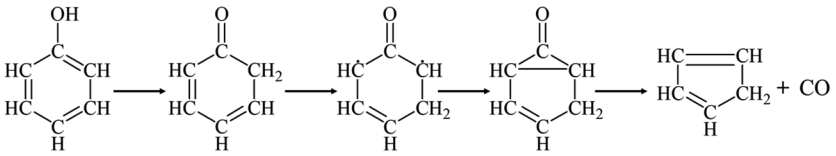

Path 1

Catechol, as the simplest model compounds of guaiacyl, was experimentally and theoretically investigated. The main products from catechol decomposition were CO and buta-1,3-diene, which were formed through the following Path 2 and Path 3.[23–26] Altarawneh *et al.*[23] calculated the decomposition reactions of catechol, and found that the Path 2 was dominant at low temperature, and Path 3 was dominant at high temperature.

Guaiacol has been widely suggested as a lignin model compound in many experimental and computational studies on lignin pyrolysis. Scheer *et al.*[30] studied the unimolecular thermal decomposition of guaiacol, and directly observed cyclopentadiene formation *via* cyclohexadienone by photon ionization time-of-flight mass spectrometry and matrix isolation infrared spectroscopy (PIMS-IR). Vinylacetylene, cyclopentadienone, acetylene and hydroxy-cyclohexadienone were observed to certify the ring-opening pathway of aromatic structure in guaiacol as Path 4. The initial decomposition step is the loss of methyl radical and the hydroxy-cyclopentadienyl radical is produced by the decarbonylation of the 2-hydroxyl phenoxy radical. Nguyen *et al.*[31] comprehensively studied on detailed kinetic modeling for thermal decomposition of guaiacol which is essential to gain insights into the complicated process.

Few works were reported on the thermal decomposition of syringol, and there was limited information on the products generated from syringol. Asmadi *et al.*[34] investigated thermal reactions of guaiacol and syringol as lignin model aromatic nuclei, and focused on the role of the additional methoxyl group in the formation of coke, tar and gas. Harman-Ware *et al.*[36] reported the fast pyrolysis of the lignin monomers sinapyl and coniferyl alcohol using pyrolysis-GC/MS, and focused on the tar generated from sinapyl : guaiacyl ratios. To the best of our knowledge, there are no reports on detailed distribution of light volatile products generated from syringol decomposition.

Above all, the experimental information on detailed distribution of products such as inorganic gases (IGs) and C_1–C_5 light hydrocarbons (LHs) from the pyrolysis of monomer phenolic model compounds was still lacked, leading to the poor understanding of vapor-phase reactions during pyrolysis of solid fuel resources, especially ring-reductions of aromatic structures. In this study, three model compounds were employed to provide experimental data for future detailed simulation and to understand the vapor-phase reactions during pyrolysis of solid fuel resources. Guaiacol, syringol and phenol were pyrolyzed at 550 °C–950 °C, and 0.1 s–4.2 s, and the quantitative distribution of the products were recorded by on-line GCs. Effects of temperature, residence time and the methoxyl addition on products distribution and ring-opening reactions were discussed, focused on the formation of IGs and C_1–C_5 LHs.

2. Experimental section

2.1 Materials

Gas-phase model compounds, phenol, guaiacol and syringol, were used as phenolic representatives of structural entities in solid fuels and tar. Phenol, guaiacol and syringol were purchased from Sinopharm Chemical Reagent Co., Ltd, China. All samples were of analytical grade and used without any further purification.

2.2 Equipment and procedure

Thermal decompositions of model compounds were investigated using a tubular reactor system at temperature (550–950 °C, 0.7 s) and residence time (RT, 0.1 s–4.2 s at 650 °C and 750 °C) with an inert gas helium (He). The reactor system consisted of a vaporizer, a quartz tubular-flow reactor, and an online GC as shown in Fig. 1. First, GC was separated with the

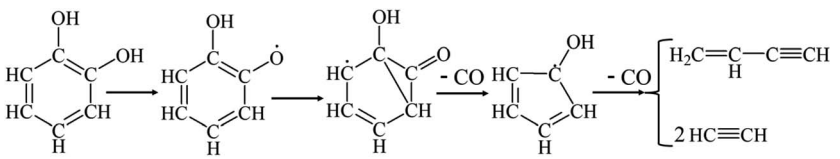

Path 2

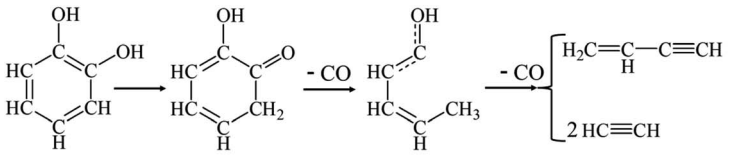

Path 3

tubular reactor by a six-way-valve, and GC baseline was stabled by carrier gas He. At the same time, keeping valves A and B closed and valve A open, He was used to exhaust air from tubular reactor. Tubular reactor was heated to expected temperature (550–950 °C) by a multi-stage furnace. After temperature and baseline were stable, tubular reactor was connected to GC by switching the six-way-valve. 1 mg sample was loaded into a Pyrex tube fixed in the vaporizer. The vaporizer was heated to 250 °C by an electric furnace to vaporize model compounds. 10 min later, valve C was closed, and valve A and B were quickly opened. Vapor of model compounds was passed from the Pyrex tube into the tubular reactor with a carrier gas (He) at 241 kPa. The quartz tubular-flow reactor was used for the decomposition of lignin model compounds in the helium atmosphere. The inner diameter of the tubular-flow reactor was 4 mm. Residence time was controlled by the heated length of reactor inserted into the multi-stage furnace. Products were carried to GC column with carrier gas, and further identified by online GCs equipped with TCD and/or FID. Three different columns were employed to analyze the products, including a 4 m long packed column with 60/80 mesh Gasukuropak 54 (GL Sciences, Co. Ltd), a 25 m long, 0.25 mm i.d. capillary column (ParaBOND Q, $d_f = 0.25$ μm, Agilent), and a 60 m long, 0.25 mm i.d. capillary column (TC-1701, $d_f = 0.25$ μm, GL Sciences, Co. Ltd). GC conditions in this study were the same as our previous publications[7,25,40] as listed in Table A1 in ESI.†

2.3 Products analysis

Products were quantified with the same method in our previous publications[7,25,40] and the peak identification can be found in publication:[7,40] (1) chromatographic peaks were identified by comparison with GC/MS peaks or by standard substances; (2) when standard substances are available, products except C_1–C_5 LHs are quantified by standard curve method; (3) when the standard substances are unavailable (C_1–C_5 LHs), methane is used as the reference substance, and the number of available carbon is used to quantify products. FID is a mass detector, so products yield can be calculated by eqn (1)–(3) below. It should be noted that carbon monoxide (CO) and carbon dioxide (CO_2) were detected by TCD, a concentration detector. Since methane can be detected by FID and TCD at the same time, methane was selected as a reference calibration factor to calculate the yield of CO and CO_2, as eqn (4). Each test ran three times, and the relative errors of the product yield generally within ±10%. The mean yield of each detectable products was illustrated in this study and used to analyze the decomposition behavior of lignin model pyrolysis.

Mass of product i, standard substances are available:

$$m_i = \frac{A_i}{\left(\frac{A_{i\text{-st}}}{N_{i\text{-st}}}\right)} \times M_i \quad (1)$$

Standard substances are unavailable:

$$m_i = \frac{A_i}{\left(\frac{A_{CH_4}}{N_{CH_4}}\right) \times R} \times M_i \quad (2)$$

Yield of product i,

$$y_i = \frac{m_i}{m_{i\text{-feed}}} \times 100\% \quad (3)$$

Yield of CO and CO_2,

$$y_{i\text{-cro}} = \frac{y_i}{\left(\frac{y_{CH_4\text{-TCD}}}{y_{CH_4\text{-FID}}}\right)} \quad (4)$$

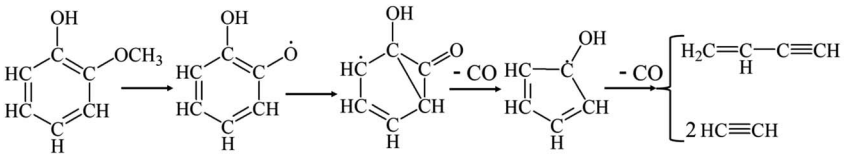

Path 4

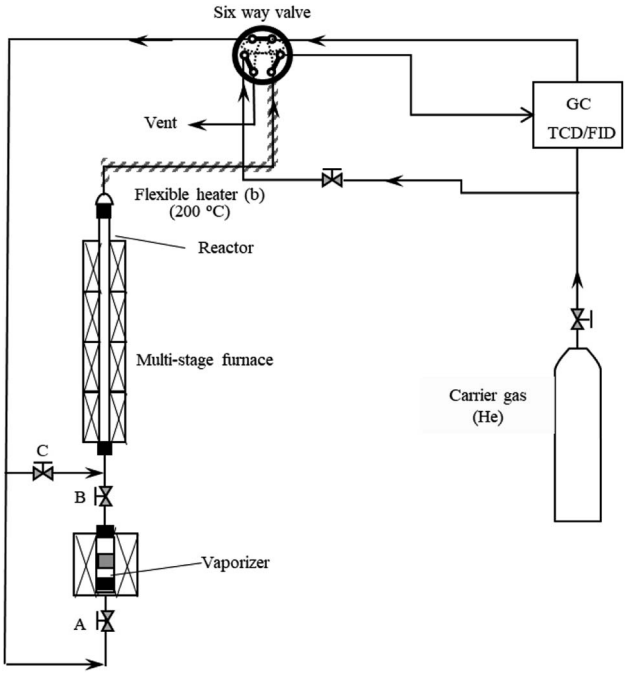

Fig. 1 Schematic representation of the experimental set-up for thermal decomposition.

In these equations, m_i denotes the mass of product i; $m_{i\text{-feed}}$ denotes the mass of feed guaiacol; A_i denotes the peak area of product i; $A_{i\text{-st}}$ denotes the peak area of standard substances i; $N_{i\text{-st}}$ denotes the moles number of standard substances i; M_i denotes the mass weight of product i; R_i denotes the response factor of effective carbon number; y_i denotes the yield of product i.

3. Results and discussion

Vapor phase reactions during pyrolysis and gasification of solid carbon resources are inevitable and critical for the formation of final products. Light volatile products paly important roles in aromatic ring-formation reactions, and C_1–C_5 LHs are known to be precursors to single-ring aromatics and growth species in polycyclic aromatic hydrocarbons (PAH) buildup reactions.[7,40–45] Published papers have reported ring-reduction/CO elimination to generate C_1–C_5 radicals and/or fragments are dominate decomposition pathways of phenolic compounds.[21–38] Our previous work[25] in this series has reported the identification of 54 species from *o*-, *m*- and *p*-benzenediol with the same analysis techniques used in this work. Concerning ring-reduction/CO elimination, mechanisms for three benzendiol-isomers decomposition and formation of the C_1–C_5 light hydrocarbons (C_1–C_5 LHs) have been discussed based on the distribution of 54 species in our previous study.[25] Actually, primary products generated from solid carbon resources (especially lignin) are phenol-type compounds with methoxyl (OCH_3). An understanding of the effects of OCH_3 on the products distribution is essential to interpret the decomposition mechanism of phenolic compounds. Hence, this study investigated the thermal decomposition of phenol, guaiacol and syringol as three phenolic compound representatives of structural entities in solid carbon resources, and mainly focused on the distributions and formation of light volatile decomposition products. All detected products in this study were clarified into five groups as IGs, C_1–C_5 LHs, light oxygenated compounds (LOCs), aromatic hydrocarbons (AHs) and phenols (PHLs). Conversion rate and main products distributions were quantified to examine the effect of temperature, residence time (RT) and OCH_3 on the thermal behavior of phenolic compounds. Thermal behavior of phenolic compounds and formation

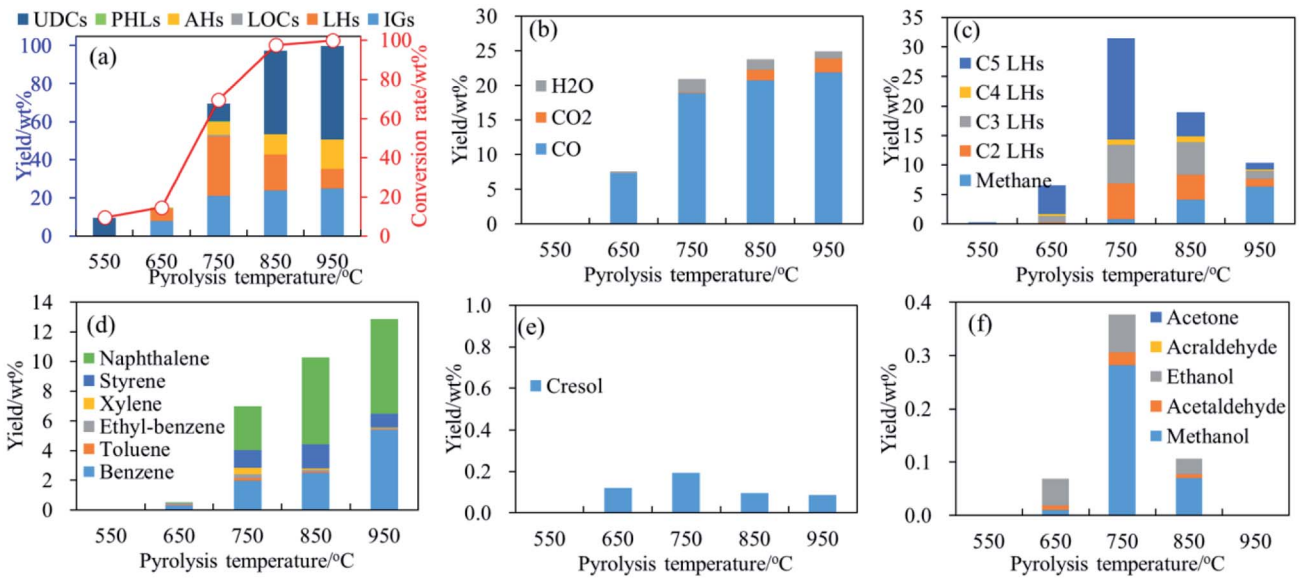

Fig. 2 Conversion rate and products distribution of phenol decomposition at 400–950 °C, 0.7 s. (a) Conversion rate and products distribution; (b) IGs; (c) C_1–C_5 LHs; (d) AHs; (e) PHLs; (f) LOCs.

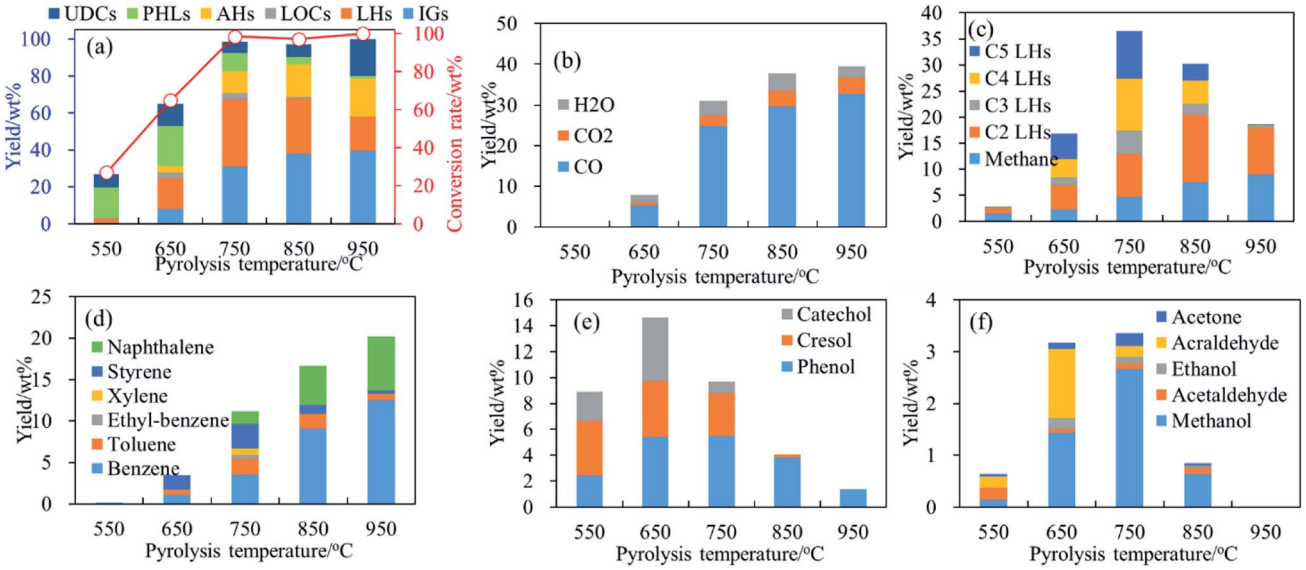

Fig. 3 Conversion rate and products distribution of guaiacol decomposition at 400–950 °C, 0.7 s. (a) Conversion rate and products distribution; (b) IGs; (c) C_1–C_5 LHs; (d) AHs; (e) PHLs; (f) LOCs.

mechanism of light volatile products will be discussed based on the experiment results.

3.1 Effect of temperature on conversion rate and products distribution

Fig. 2–4, respectively, present the conversion rate and yields of main products generated from pyrolysis of phenol, guaiacol and syringol as functions of temperature. In the temperature range of 550 °C–950 °C, noticeable differences on conversion rate and product yields reveal temperature strongly affects the thermal behavior of phenolic compounds and the formation of light volatile products. Temperature effects on pyrolysis of phenol, guaiacol and syringol are discussed, respectively, in the following parts.

3.1.1 Phenol. Fig. 2(a) shows that conversion rate of phenol is very low at 550 °C and no light-volatile-products are detectable by online GC. Phenol is converted rapidly at temperatures ≥650 °C, and completely converted at temperatures ≥850 °C. Ring-reduction/CO elimination (Path 1) was reported as the main phenol decomposition pathway to support the formation of CO and C_5 LHs (especially cyclopentadiene).[21] The observed

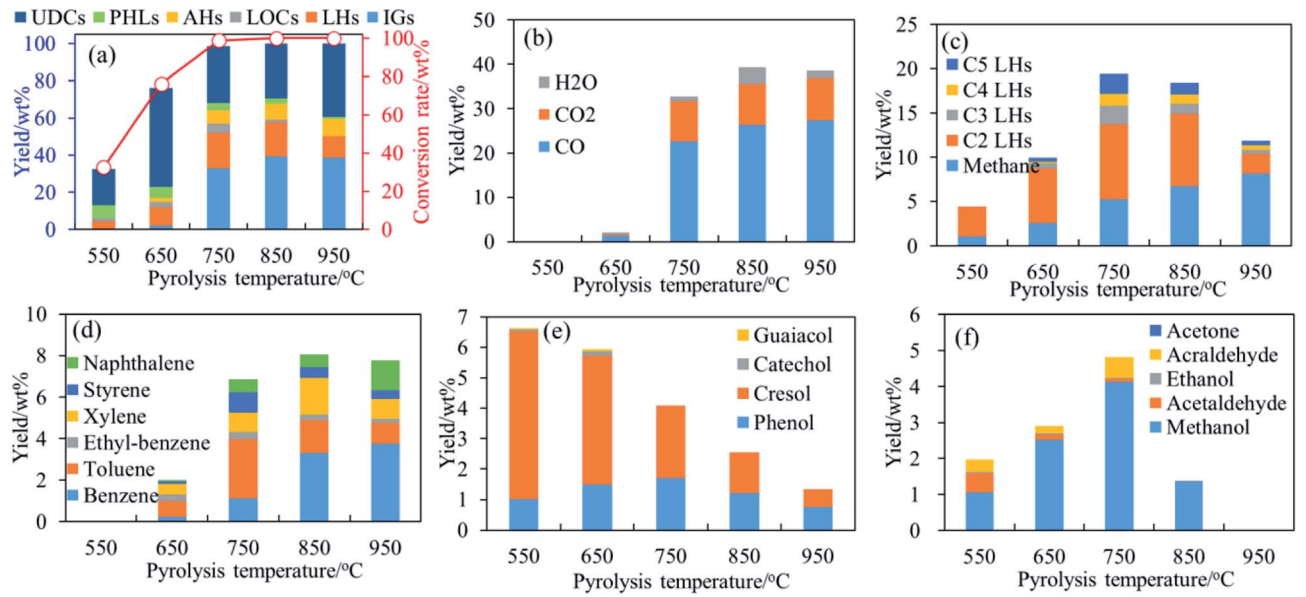

Fig. 4 Conversion rate and products distribution of syringol decomposition at 400–950 °C, 0.7 s. (a) Conversion rate and products distribution; (b) IGs; (c) C_1–C_5 LHs; (d) AHs; (e) PHLs; (f) LOCs.

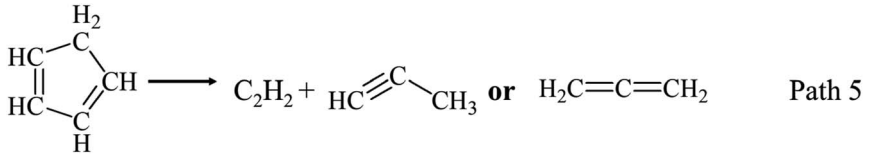

effect of temperature on CO yield in Fig. 2(b) is consistent with conversion rate of phenol exhibited in Fig. 2(a). CO yields sharply increase from 7.25 wt% at 650 °C to 18.84 wt% at 750 °C, followed by a slow increase of yield to 21.91 wt% with temperature increasing to 950 °C. C_5 LHs yields also increase sharply from 5.93 wt% at 650 °C to 17.16 wt% at 750 °C as shown in Fig. 2(b). The results of CO and C_5 LHs indicate that ring-reduction/CO elimination during phenol pyrolysis happens dramatically at temperatures ≥750 °C.

Fig. 2(c) shows C_5 LHs yield decreases with temperature increasing from 750 °C to 950 °C. Considering the structure of phenol, C_1–C_4 LHs products are possibly formed from the rupture of C_5 LHs. As illustrated in Fig. 2(c), yields of C_1–C_4 LHs are much lower than C_5 LHs at 650 °C and 750 °C. Yields of methane (CH_4) increase to 6.33 wt% with temperature increasing to 950 °C. C_2 LHs and C_3 LHs have similar distribution trends with C_5 LHs, and their maximum yield, achieved at 750 °C, were 6.18 wt% and 6.54 wt%, respectively. The rupture of C_5 LHs as Path 5 can support the formation of C_2 LHs and C_3 LHs.[21,24] C_4 LHs yields are the lowest in C_1–C_5 LHs, which was possibly formed by the combination of two C_2 LHs, or the rupture of C_5 LHs with a C_1 radical/fragment elimination.

Another consumption pathway of C_5 LHs is to support the formation of heavy-weight-molecular products such as AHs and coke. In this work, main detected AHs generated from phenol decomposition are benzene, naphthalene, and styrene as shown in Fig. 2(d). Cyclopentadiene was reported as an important precursor to naphthalene as path 6,[7,44] which can explain the increasing yield of naphthalene, as illustrated in Fig. 2(d), at temperatures ≥750 °C.

Benzene yields are lower than naphthalene, and monotonously increase in the temperature region of 750 °C–950 °C. Benzene is possibly formed by H-substitution reaction of OH[30,31] or the combination of C_1–C_5 LHs as Path 7–9.[7,25,40] Styrene was possibly formed by the combination of C_4 LHs and/or C_2 LHs,[41–43] and the temperature of peak yield is 850 °C. With temperature increasing, the decrease in styrene yield reveals styrene was possibly involved in the formation of PAH and coke at temperatures ≥850 °C.

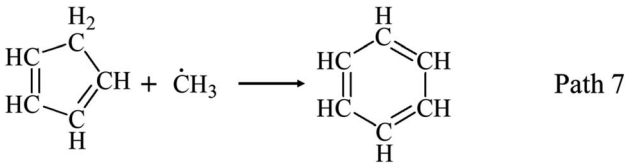

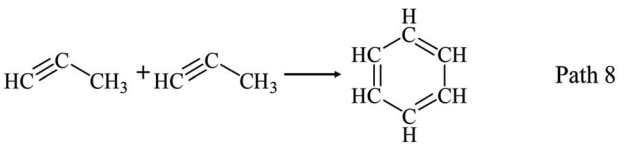

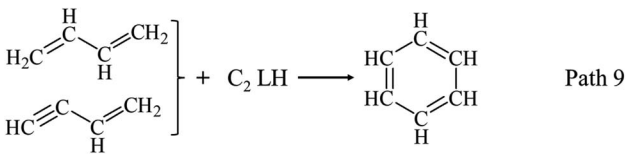

In addition, CO_2 and H_2O are also detected with a much lower yield than CO, as illustrated in Fig. 2(b). Yields of CO_2 increase with temperatures and get its maximum (1.96 wt%) at 950 °C. Yields of H_2O increase from 0.30 wt% to 2.03 wt% with temperatures increasing from 550 °C to 750 °C, and then reduce as shown in Fig. 2(b). As shown in Fig. 2(e) and (f), yields of cresol and LOCs are very low. Main detected PHLs is cresol, and its peak yield is achieved at 750 °C as shown in Fig. 2(e). Main

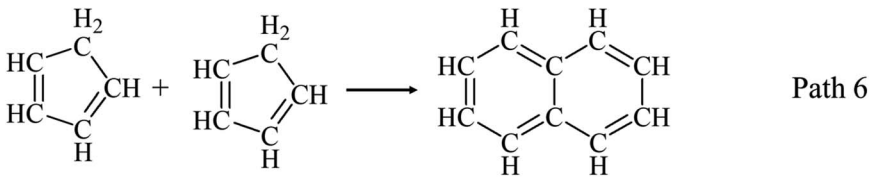

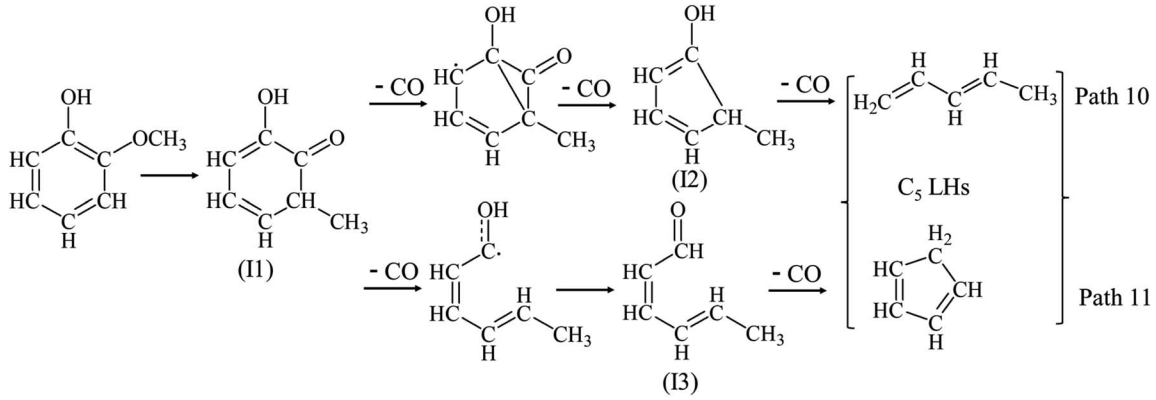

LOCs are methanol, ethanol and acetaldehyde, and the sum yields of LOCs are lower than 0.5 wt% as shown in Fig. 2(f). Yields of methanol get its maximum at 750 °C.

3.1.2 Guaiacol. Guaiacol pyrolysis were conducted in the temperature region of 400 °C–950 °C. Conversion rate of guaiacol at 400 °C is as low as 4.89 wt%, with the formation of phenol, cresol and catechol. Fig. 3 presents the conversion rates and yields of main products generated from pyrolysis of guaiacol as functions of temperature 550 °C–950 °C. Conversion rates of guaiacol increase from 26.88 wt% at 500 °C to 98.47 wt% at 750 °C as shown in Fig. 3(a), and guaiacol is almost completely decomposed above 750 °C. Product components and distributions vary with temperatures obviously as illustrated in Fig. 3(a). Fig. 3(a) reveals that PHLs are main products below 650 °C, while IGs, LHs and AHs are main product components above 650 °C. UDCs yields increase from 7.39 wt% at 550 °C to 11.90 wt% at 650 °C, and then reduce to 6.20 wt% at 750 °C. UDCs yields increase again to 20.13 wt% at temperature >750 °C. The increasing high yields of UDCs above 750 °C are possibly explained by the formation of PAHs and coke. In this study, black coke is observed on the reactor-wall during guaiacol pyrolysis at temperatures ≥750 °C. No coke is observed at 550 °C and 650 °C. Components of UDCs at 550 °C and 650 °C would be some oxygenated intermediates formed from guaiacol decomposition. Those oxygenated intermediates are quickly decomposed to support the formation of IGs and LHs at 750 °C, leading to the obviously increasing yield of IGs and LHs at 750 °C as shown in Fig. 3(a).

Even though the thermochemistry of the guaiacol is not well-known, the initiation reaction during the decomposition of guaiacol is most likely to be the scission of an OCH_3 to form methyl (CH_3) and hydroxyphenoxyl radical in Path 4.[30] CH_3 combined with a hydrogen supports the formation of CH_4 which yields increase to 8.88 wt% with temperatures increasing to 950 °C. At high temperature CH_4 is also formed from the rupture of C_2–C_5 LHs.

Ring-reduction/CO elimination (Path 4) of hydroxyphenoxyl radical was proposed by Scheer *et al.*[30] based on the detection of hydroxycyclopentadienyl radical, cyclopentadienone and acetylene and vinylacetylene by photoionization time-of-flight mass spectroscopy. Concerning ring-reduction/CO elimination as Path 4, CO, C_2 LHs and/or C_4 LHs are expected from guaiacol pyrolysis in this study. Fig. 3(b) shows CO is the absolutely dominated product from guaiacol pyrolysis. CO is detected at temperatures as low as 500 °C, even though its yield is as low as 0.01 wt%. CO yields largely increase to 32.75 wt% in temperature region of 650 °C–950 °C. C_2 LHs and C_4 LHs are two of main products from guaiacol pyrolysis. C_4 LHs yields increase from 0.09 wt% to 10.01 wt% with temperatures increasing from 550 °C to 750 °C, and then reduce to 0.20 wt% at higher

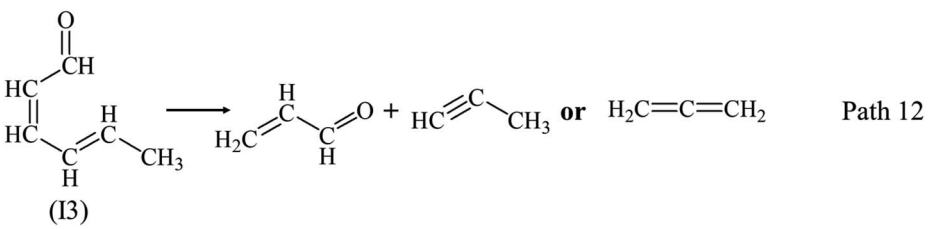

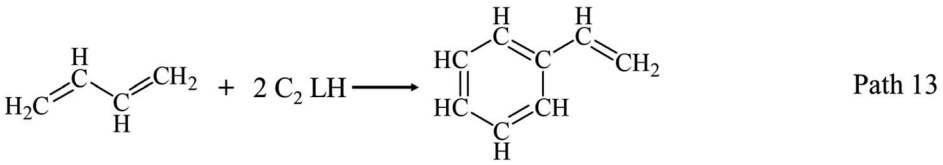

Path 13

temperatures. Decreases of C_4 LHs yield are possibly caused by the formation of C_2 LHs or heavy-weight molecular products. C_2 LHs present similar trends, as functions of temperature, with C_4 LHs. C_2 LHs' temperatures of peak yield shift to 850 °C as its yields decrease at higher temperatures. The distributions of CO, C_2 LHs and C_4 LHs can testify Path 4 proposed by Scheer *et al.*[30]

Fig. 3(c) reveals that C_5 LHs are another main LHs from guaiacol pyrolysis, which yields have same trend as functions of temperature with C_4 LHs. Phenol is also detected from guaiacol pyrolysis with a maximum yield (5.46 wt%) at 650 °C. Hence, as discussed in Section 3.1.1, C_5 LHs can be formed form the phenol decomposition. However, the low yield of phenol cannot support the high yield of C_5 LHs. In analogy to catechol decomposition as Path 3, the guaiacol decomposition would also be started with the CH_3 migration to a neighbor carbon to form intermediate (I1). In analogy to Path 2 and Path 4, intermediate (I1) can be converted to C_5 LHs by the ring-reduction reaction/CO elimination *via* intermediates (I2, methylcyclopentenol) as Path 10. In analogy to Path 3, intermediate (I1) also can be converted by a ring-reduction reaction/CO elimination *via* intermediates (I3) to produce CO and C_5 LHs as Path 11. Intermediate (I2) also possibly supports the formation of acraldehyde and C_3 LHs as Path 11. Fig. 3(f) illustrates the profile of acraldehyde yield *vs.* temperature from guaiacol pyrolysis. Acraldehyde gets its peak yield at 650 °C, and then is decomposed to CO/CO_2 and C_2 LHs at higher temperature. C_3 LHs show the lowest yield among C_1–C_5 LHs at all temperatures, formed by Path 12 or Path 5.

AHs yields increase obviously above 650 °C as shown in Fig. 3(a) and (d), and get its maximum (20.43 wt%) at 950 °C. Fig. 3(d) shows benzene and naphthalene are two main components in AHs, and their yields increase with temperatures increasing to 950 °C. Benzene and naphthalene can be formed as discussed in Section 3.1.1 by the combination of C_1–C_5 LHs. Styrene has a higher yield than other AHs at 650 °C, and achieves its maximum yield (3.00 wt%) at 750 °C. Considering the distribution of C_2 and C_4 LHs, styrene can be produced by the combination of C_2 and C_4 LHs as Path 13–Path 15.[40–45] Toluene has a low yield and achieves its maximum yield (1.90 wt%) at 750 °C.

Fig. 3(e) shows the yield of PHLs as functions of temperature. Guaiacol is mainly converted to PHLs (mainly phenol, cresol, and catechol) at 400 °C and 500 °C. PHLs yields get its maximum at 650 °C, and then reduce above 750 °C. Phenol gets its maximum yield at 650 °C. It is often thought to be formed by the H-substitution of methoxy groups. Another pathway for the radical/radical recombination was proposed by Scheer *et al.* to explain the formation of phenol as Path 16.[30] At the same time, intermediate (I2) can be also formed from guaiacol decomposition as Path 10 as discussed above, which can promote the formation of phenol as Path 16.

Fig. 3(e) reveals catechol is one of main PHLs generated by the combination of hydroxyphenoxyl radical and hydrogen radical. Maximum yield of catechol is achieved at 650 °C, and consumed rapidly at temperatures ≥750 °C. Catechol decomposition has been investigated and supported the formation of CO and buta-1,3-diene *via* H-migration to neighbor carbon and ring-reduction reactions as Path 2 and Path 3. LOCs exist with its sum yield being 3.17 wt% at 650 °C, and 3.35 wt% at 750 °C as shown in Fig. 3(f). Less than 1.00 wt% LOCs are detected at 500 °C and above 850 °C. LOCs are mainly methanol, acraldehyde and acetone. Methanol and acetone get its maximum yield at 750 °C, while acraldehyde achieves its maximum yield at 650 °C. With temperatures increasing, LOCs can be decomposed to IGs and LHs, leading to the reduction of yield at high temperatures.

In addition, CO_2 yields increase from 0.75 wt% at 650 °C to 3.97 wt% at 950 °C, which are much lower than CO yield. H_2O

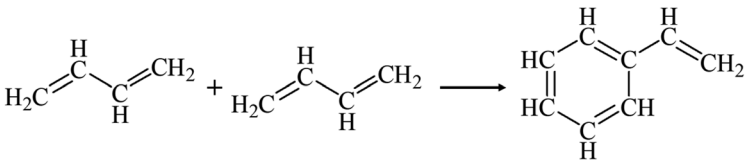

Path 14

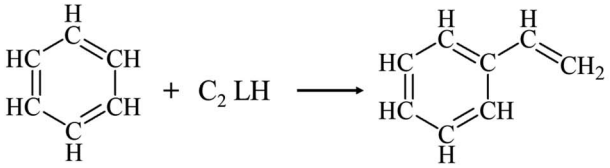

Path 15

yields increase with temperatures, and get its maximum yield (4.27 wt%) at 850 °C. The formation of CO_2 will be discussed in Section 3.3.

3.1.3 Syringol. Syringol pyrolysis was less investigated in published works, and the decomposition mechanism is still unclear. In this study, syringol was pyrolyzed to investigate the distributions of light volatile products considering the effects of OCH_3. Conversion rate and yield profiles of products as functions of temperature are illustrated in Fig. 4. Fig. 4(a) reveals conversion rates of syringol increase quickly to 94.74 wt% in the temperature region of 550 °C–750 °C, and is almost completely converted above 750 °C. Because of the low bond dissociation energy, similarly with guaiacol, the initiation reaction of syringol decomposition is most likely the scission of OCH_3 to form CH_3 and hydroxyphenoxyl radicals (loss of one or two CH_3). In analogy to Path 4 of guaiacol, ring-reduction/CO elimination of hydroxyphenoxyl radicals is possibly one decomposition way of syringol. Product components and distributions vary with temperature obviously as illustrated in Fig. 4(a). Main detected products are IGs and C_1–C_5 LHs. Concerning ring-reduction/CO elimination, CO and C_1–C_5 LHs are firstly concerned and illustrated in Fig. 4(b) and (c). Sum yields of IGs increase dramatically at temperatures ≥750 °C. As illustrated in Fig. 4(b), CO is dominant IGs generated from syringol pyrolysis. Yields of CO sharply increase from 1.3 wt% at 650 °C to 22.57 wt% at 750 °C, and then slowly increase to 27.44 wt% at temperatures above 750 °C. This result can prove the existence of CO elimination during syringol pyrolysis, and CO elimination happened obviously at 750 °C. Fig. 4(c) shows sum yields of LHs largely increase from 4.4 wt% at 550 °C to 19.38 wt% at 750 °C, and then reduce to 10.30 wt% with temperatures increasing to 950 °C. Different from phenol and guaiacol, CH_4 and C_2 LHs are two main LHs generated from syringol pyrolysis. Obviously shown in Fig. 4(c), CH_4 and C_2 LHs have a much higher yield than C_3–C_5 LHs. CH_4 yields increase to 8.13 wt% with temperatures increasing to 950 °C. C_2 LHs are mainly ethyne, ethene, and ethane, and achieve its maximum sum yield at 750 °C. CH_3 combined with a hydrogen radical or another CH_3 support the formation of CH_4 and ethane, leading to the high yield of CH_4 and ethane. With temperatures increasing, ethyne and ethene can be formed from ethane with the loss of H. Yields of C_3–C_5 LHs are lower than 2.5 wt%, and achieve their maximum at 750 °C. In analogy to guaiacol, ring-reduction/CO elimination as Path 17 would be a source of C_3 LHs and CO. Lower yields of C_3 LHs indicate Path 17 happened with a low probability. It is also possible the carbon–oxygen linkages in two OCH_3 are broken at the same time, as Path 18, and give the intermediate (I12). Intermediate (I12) is unstable, and easily decomposed to CO and C_1 fragments such as methylene (CH_2) and methenyl (CH), methane, methanol or formaldehyde. Path 18 can explain the formation of C_1–C_2 LHs. The detailed reactions of syringol decomposition still need to be investigated experimentally and theoretically in future work.

With temperatures increasing, main detected AHs generated from syringol pyrolysis are benzene, toluene, xylene, ethylbenzene, naphthalene, and styrene as shown in Fig. 4(d). Yields of benzene increase to 3.76 wt% with temperatures increasing to 950 °C. Toluene achieves its maximum yield (2.85 wt%) at 750 °C, while xylenes achieve its maximum yield (1.78 wt%) at 850 °C. Toluene and xylenes are possibly formed by CH_3-substitution reaction of OH or OCH_3 and the combination of C_1–C_5 LHs. Styrene achieves its maximum yield at 750 °C during syringol pyrolysis. Yields of naphthalene increase to 1.43 wt% with temperatures increasing to 950 °C. Main detected PHLs are cresol and phenol. Yields of cresol are much higher than phenol. Cresol achieves its maximum yield at 550 °C, and is

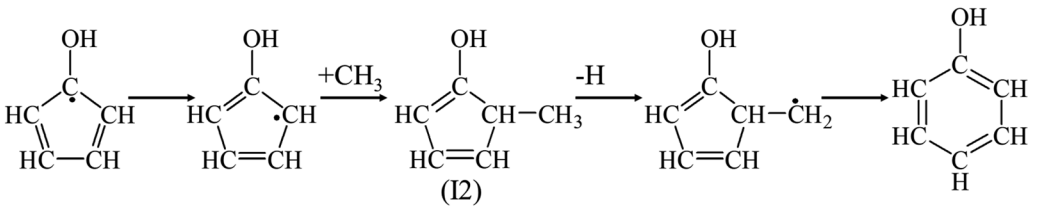

Path 16

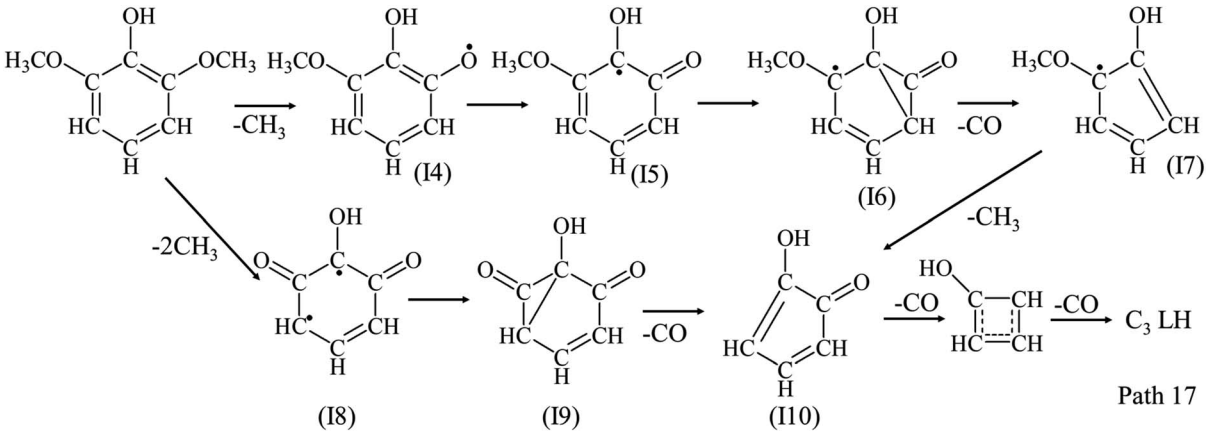

decomposed quickly with temperatures increasing as shown in Fig. 4(e). Phenol gets its maximum yield at 650 °C as shown in Fig. 4(e). Main LOCs are methanol, acraldehyde, and acetaldehyde as shown in Fig. 4(f). Yields of methanol and acraldehyde get its maximum at 750 °C. Acetaldehyde gets its maximum yield at 550 °C, and is decomposed quickly with temperatures increasing as shown in Fig. 4(f).

Yields of CO_2 increase monotonously to 9.55 wt% in the temperature region of 650 °C–950 °C. Yields of H_2O increase from 0.51 wt% to 3.62 wt% with temperatures increasing to 850 °C, and then reduce as shown in Fig. 4(b).

3.2 Effect of residence time on conversion rate and products distribution

During pyrolysis of phenolic compounds, ring reduction/CO elimination to form IGs and C_1–C_5 LHs occurred at 650 °C and dramatically at 750 °C. At these temperatures less C_1–C_5 LHs are consumed for the formation of AHs and/or coke. Hence, effects of RT on the thermal behavior of phenolic compounds were examined by guaiacol pyrolysis in RT region of 0.1–4.2 s at 650 °C and 750 °C. Conversion rate and main products distributions generated from guaiacol pyrolysis are illustrated in Fig. 5 and 6.

Conversion rates of guaiacol increase to 93.50 wt% with RT at first 1.4 s, and guaiacol is almost completely decomposed after 1.4 s at 650 °C as shown in Fig. 5(a). Yields of all products increase with RT as shown in Fig. 5(a). Main PHLs are catechol, cresol and phenol as shown in Fig. 5(b). With RT increasing from 0.1 s to 4.2 s, yields of phenol and cresols increase to 9.49 wt% and 4.83 wt%, respectively, at 650 °C. Catechol gets its maximum yield at 1.4 s, and then is converted to CO and C_4 LHs. LOCs at 650 °C are mainly methanol and acraldehyde, and yields of methanol and acraldehyde increase to 2.39 wt% and 2.47 wt%, respectively, with RT increasing to 4.2 s as shown in Fig. 5(c). IGs yields increase from 2.54 wt% to 17.97 wt% at 650 °C with RT increasing from 0.1 s to 4.2 s, and Fig. 5(d) illustrates the yields of CO, CO_2 and H_2O with RT. CO yields increase from 1.80 wt% to 15.01 wt% with RT at 650 °C, while yields of CO_2 and H_2O increase slightly with RT and much lower than yield of CO at 650 °C. At 650 °C, C_1–C_5 LH yields except C_2H_6 increase in the region of 0.1 s–4.2 s, while C_2H_6 gets its maximum yield at 0.7 s as shown in Fig. 5(e). Fig. 5(f) illustrates the yield of benzene, toluene and styrene with RT at 650 °C, and their yields all increase in the region of 0.1 s–4.2 s.

Fig. 6 illustrates conversion rate and products distribution of guaiacol pyrolysis at 750 °C. Guaiacol was decomposed quickly,

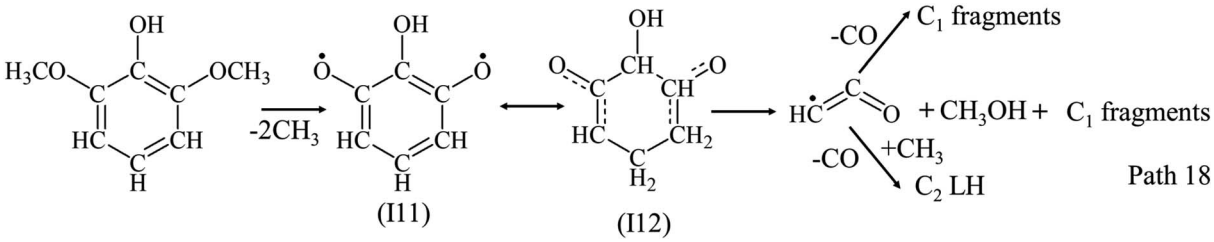

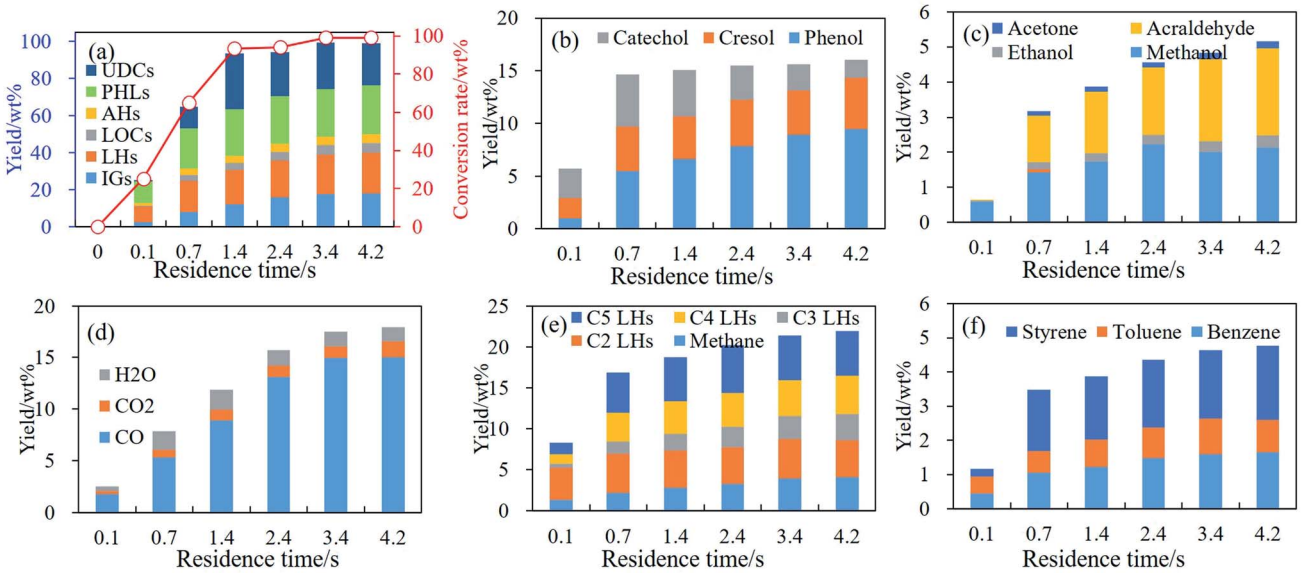

Fig. 5 Conversion rate and products distribution of guaiacol decomposition at 650 °C, 0.1–4.2 s. (a) Conversion rate and products distribution; (b) PHLs; (c) LOCs; (d) IGs; (e) C_1–C_5 LHs; (f) AHs.

and conversion rate is more than 95 wt% at 750 °C, 0.1 s–4.2 s. Main products are IGs, C_1–C_5 LHs and AHs as illustrated in Fig. 6(a). Yields of IGs, C_1–C_5 LHs and AHs increase with RT, while yields of PHLs and LOCs reduce obviously with RT as shown in Fig. 6(a). Fig. 6(b) shows yields of phenol and cresol at 750 °C is lower than those at 650 °C, which achieve its maximum value at 0.7 s. Yields of catechol reduce with RT at 750 °C. As discussed above, at 750 °C, decomposition of phenolic compounds occurred to form CO and C_1–C_5 LHs through ring-reduction/CO elimination reactions.[21–38] Hence, yields of PHLs reduce with RT increasing in the region of 0.7 s–4.2 s. LOCs yields reduce with RT at 750 °C, and methanol and acraldehyde are main LOCs as shown in Fig. 6(c). Methanol is formed quickly at 750 °C, and its yields slightly vary between 2.17 wt% and 2.67 wt% in RT region of 0.1 s–4.2 s. Acraldehyde is formed quickly at first 0.1 s, and decomposed quickly after 0.7 s. Path 12 of intermediate (I3) can be proved by the existence of acraldehyde. Hence, Path 11 is possible with a CH_3 migration to a neighbor carbon, which is followed by the ring-reduction reaction to produce CO and C_5 LHs during guaiacol pyrolysis.

Much higher yields of IGs and C_1–C_5 LHs at 750 °C than those at 650 °C indicate that ring-reduction/CO elimination

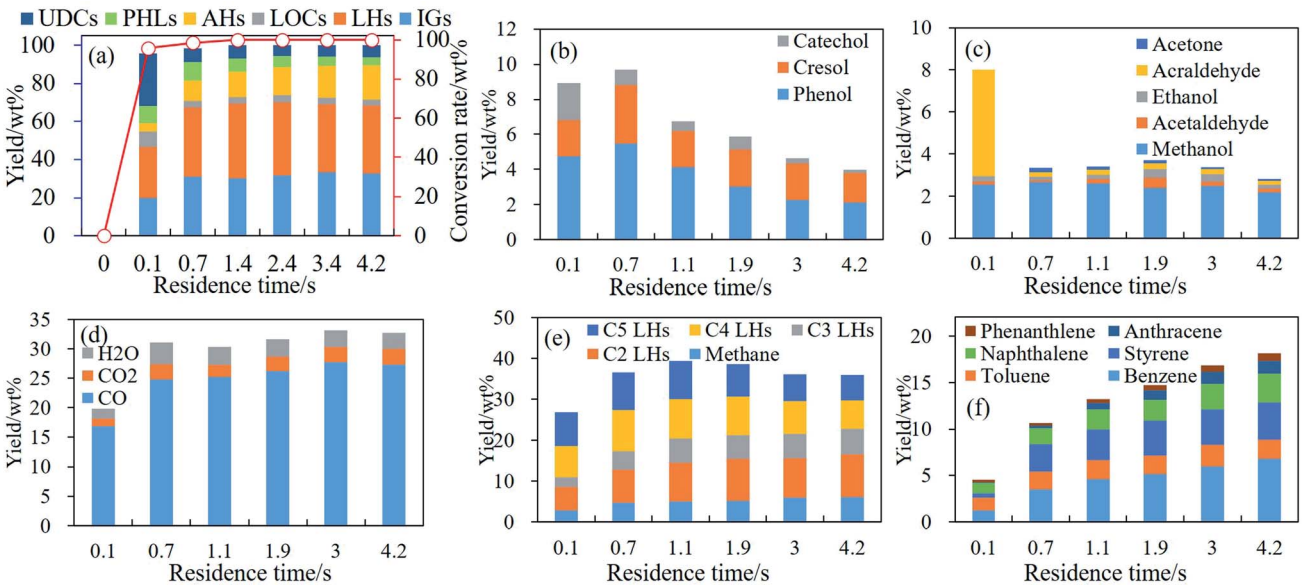

Fig. 6 Conversion rate and products distribution of guaiacol decomposition at 750 °C, 0.1–4.2 s. (a) Conversion rate and products distribution; (b) PHLs; (c) LOCs; (d) IGs; (e) C_1–C_5 LHs; (f) AHs.

Table 1 The conversion starting temperature, the temperature of conversion rate higher than 95 wt%, and the main products from phenol, guaiacol and syringol

	Phenol	Guaiacol	Syringol
Conversion starting temperature	650 °C	550 °C	550 °C
Conversion rate >95% temperature	850 °C	750 °C	750 °C
CO/wt%	21.91	32.75	27.44
CO_2/wt%	1.96	3.97	9.55
Main C_1–C_5 LHs	$C_5 > C_2 > C_3$	$C_4 > C_5 \approx C_2$	$C_2 > C_1$
Main AHs	Naphthalene, benzene	Benzene, styrene	Benzene, toluene, xylene
Main LOCs	—	Methanol, acraldehyde	Methanol
Main PHLs	—	Catechol, cresol, phenol	Cresol, phenol

reactions of guaiacol are drastic at 750 °C. Fig. 6(d) illustrates the yields of CO, CO_2 and H_2O. CO yields increase from 16.94 wt% to 27.72 wt% with RT increasing, while CO_2 yields just slightly increase from 1.22 wt% to 2.72 wt% with RT from 0.1 s to 4.2 s at 750 °C. H_2O gets its maximum yield at 0.7 s, and then reduces. C_1–C_5 LHs yields at 750 °C are illustrated in Fig. 6(e), and much higher than those at 650 °C. LHs sum yields increase with RT increasing from 0.1 s to 1.1 s, and then slightly reduce with RT to 4.2 s at 750 °C. At 750 °C, methane, ethyne, ethene, ethane, propane, propene, propyne, propadiene,1-butene-3-yne, 1,3-butadiene, cyclopentadiene, 1,4-pentadiene and 1,2-pentadiene are the main LHs at 750 °C. As shown in Fig. 6(e), yields of methane, ethyne, ethene, propane, propene, and propyne increase monotonously with RT, while yields of ethane slightly reduce monotonously with RT. C_4 LHs (1-butene-3-yne and 1,3-butadiene) and C_5 LHs (cyclopentadiene, 1,4-pentadiene and 1,2-pentadiene) get their maximum yields at 0.7 s or 1.1 s, and then reduce with RT.

AHs are largely formed with a much higher yield at 750 °C than at 650 °C. Yields of main AHs compounds are illustrated in Fig. 6(f). Benzene, styrene, and naphthalene are three AHs from guaiacol pyrolysis at 750 °C, and their yields all increase with RT. As published reports, AHs can be formed by the combination of C_1–C_5 LHs. Benzene is possibly formed by H-substitution reactions of OH or OCH_3, and/or the combinations of C_1–C_5 LHs, while styrene is possibly formed by the combinations of C_4 LHs and/or C_2 LHs. Naphthalene is formed by the combinations of two cyclopatadienes, the combinations of buta-1,3-diene with benzene, or the combinations of C_2 LHs with styrene. Anthracene and phenanthlene are also detected at 750 °C, and their yields increase to 1.34 wt% and 0.82 wt% with RT at 750 °C, respectively.

3.3 Effect of methoxyl on conversion rate and products distribution

Table 1 illustrates the conversion starting temperature, the temperature of conversion rate higher than 95 wt%, and the main products from phenol, guaiacol and syringol. Phenol is converted rapidly at temperature higher than 650 °C, and completely converted above 850 °C as shown in Table 1. Guaiacol and syringol was converted rapidly at temperature higher than 550 °C, and completely converted above 750 °C. Carbon–oxygen bond in methoxyl group was easier to break than that in hydroxyl group, so the addition of OCH_3 reduced the conversion temperature, and promoted the conversion of model compounds.

Yields of UDCs at low temperatures (550 °C and 650 °C) increase in the order of phenol < guaiacol < syringol. The additional OCH_3 was easy to form phenoxy radicals in syringol and provided more opportunity for the formation of heavy molecular products such as dipolymer and tar. Yield of UDCs at 850 °C–950 °C increased in the order of guaiacol < syringol < phenol. More UDCs generated from syringol than guaiacol would be explained by the formation of large amount of coke, which was observed on the reactor-wall during syringol decomposition in this study. This was consistent with the study of Asmadi *et al.*,[34] who pyrolyzed syringol and guaiacol as lignin model compounds. They found that coke and gas (especially CH_4 and CO_2) formation was more extensive in syringol, and the additional OCH_3 was easy to form phenoxy radicals in syringol and provided more opportunity for the formation of soot.

The detected products generated from model compounds pyrolysis are IGs, LHs, AHs and PHLs as shown in Fig. 2–4 and Table 1. Oxygen content increases in the order of phenol < guaiacol < syringol, whereas maximum yields of IGs increase in

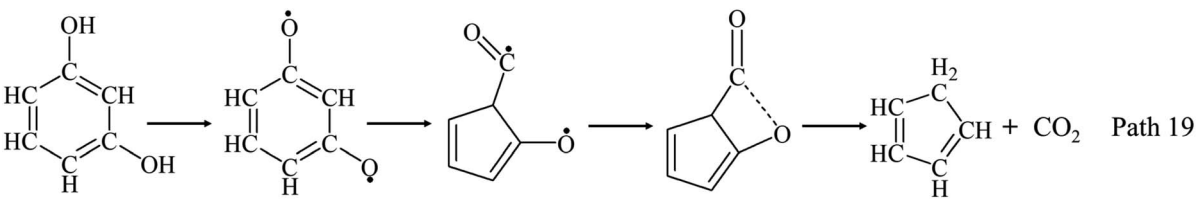

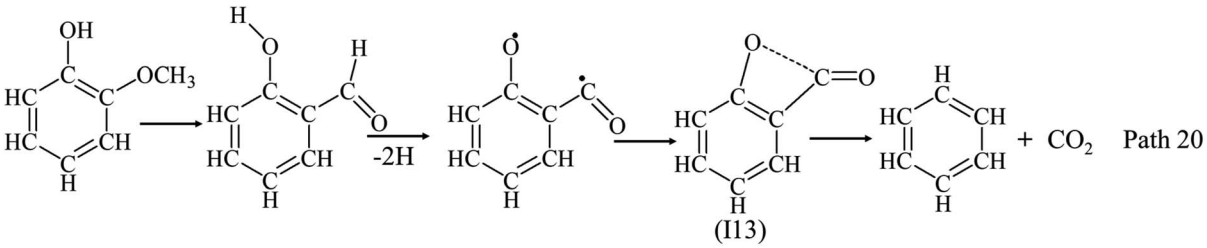

the order of phenol < syringol < guaiacol. Yields of CO and CO_2 generated from phenol, guaiacol and syringol all increase with temperature from 650 °C to 950 °C as shown in Fig. 2–4. CO is formed from ring reduction/CO elimination reactions of phenolic compounds. CO_2 can be formed by water–gas shift reaction as $CO + H_2O \rightarrow CO_2 + H_2$. As listed in Table 1, yields of CO increase in the order of phenol < syringol < guaiacol, while yields of CO_2 increase in the order of phenol < guaiacol < syringol. Yield trend of CO_2 is not consistent with CO. Water–gas shift reaction is not enough to support the formation of CO_2. Table 1 reveals that the additional OCH_3 promotes the formation of CO_2. There would be a pathway for the formation of CO_2, competing with the formation of CO, and leading to the lower yield of CO from syringol than guaiacol. Furatani *et al.*[46] calculated a reaction pathway of resorcinol for the formation of CO_2 with a four-member ring as Path 19.

In analogy to Path 19, Path 20 possibly explains the formation of CO_2 from guaiacol and syringol. The OCH_3 is converted to formyl group by concerted reaction,[32–34,47] followed by the formation of benzoyl group. Similarly with the calculation by Furatani *et al.*,[46] the benzoyl group provides a chance to form a four-member ring as intermediate (I13) in Path 19. Then, intermediate (I13) is decomposed to benzene and CO_2. Syringol has a double opportunity for the formation of CO_2, and thus has a higher yield of CO_2 than guaiacol.

Distributions of C_1–C_5 LHs are very different from each model compounds as illustrated in Table 1. Differences in the C_1–C_5 LHs distribution indicate that the ring-reduction pathways of aromatic structure are affected by the additional of OCH_3. Main LHs produced from phenol decomposition are C_5 LHs with its maximum yield (17.16 wt%, mainly cyclopentadiene) at 750 °C as shown in Fig. 2(c). C_4 LHs, C_2 LHs and C_5 LHs have a higher yield than C_1 and C_3 LHs from guaiacol decomposition. Path 4 can support the formation of C_4 LHs and C_2 LHs. The guaiacol decomposition would also be started with CH_3 migration to a neighbor carbon, followed by the ring-reduction reactions *via* intermediate (I2) to produce CO and C_5 LHs as Path 10. This path can be proved by the formation of C_5 LHs, acraldehyde and C_3 LHs produced from guaiacol at 550–750 °C.

Different from phenol and guaiacol, syringol has the lowest yield of C_1–C_5 LHs among the three model compounds, and produces more C_1 and C_2 LHs than C_3–C_5 LHs as shown in Fig. 4(c). Compared with phenol and guaiacol, the addition of OCH_3 in syringol would cause large amounts of radicals and C_1 fragments (CH_3, CH_2 and CH) formed, which supported the formation of C_1–C_2 LHs as Path 17. The detailed reactions of syringol decomposition still need to be investigated experimentally and theoretically in future work.

Main detected AHs are benzene, naphthalene, styrene, toluene and xylene as shown in Fig. 2(d), 4(d) and Table 1. The formations of AHs are related with the distribution of C_1–C_5 LHs. Yields of benzene and naphthalene all increase with temperature from 650 °C to 950 °C. Yields of naphthalene increase in the order of syringol < guaiacol < phenol. The high yield of C_5 LHs in phenol pyrolysis can explain the highest yield of naphthalene in phenol pyrolysis. C_2 and C_4 LHs are important precursors for the formation of styrene. Guaiacol decomposition produces more C_2 and C_4 LHs, leading to a higher yield of styrene than phenol and syringol. Similarly, yields of benzene increase in the order of syringol < phenol < guaiacol. The addition of OCH_3 benefited the formation of toluene and xylene, and their yields increase in the order of phenol < guaiacol < syringol. The increasing yields of cresol in the order of syringol > guaiacol > phenol reveals that the addition of OCH_3 promoted the formation of cresol. Yield of cresol generated from syringol pyrolysis reduced with temperature from 550 °C to 950 °C, which is much higher than from phenol and guaiacol.

4. Conclusions

Effects of temperature, RT and OCH_3 on the distribution of light volatile products were investigated by the pyrolysis of phenol, guaiacol and syringol. Conversion rates were increased with temperature and RT, and the addition of OCH_3 promote the decomposition of phenolic compounds at low temperature. The distribution of main products (IGs, LHs, LOCs, PHLs and AHs) from the three model compounds were recorded, respectively, with temperature and RT. IGs yields increased with temperatures and RT. CO was the dominant product, and its yields increased with temperatures and RT. Yields of C_2–C_5 LHs increased obviously at 650 °C and 750 °C, and reduced to support the formation of AHs and coke at high temperature. Ring-reduction/CO elimination reactions of phenolic compounds was an important pathway of phenolic compounds to support the formation of CO and C_1–C_5 LHs. Ring-reduction/CO elimination reactions happened at 650 °C, and drastically

above 750 °C. With the effect of OCH_3, distributions of C_1–C_5 LHs were very different, and ring-reduction reactions of phenolic compounds were significantly affected by the addition of OCH_3: ring-reduction/CO elimination reactions of phenol generated CO and C_5 LHs (mainly cyclopentadiene) *via* cyclohexadienone. Because of low bond dissociation energy of OCH_3, the thermal decomposition of the guaiacol and syringol is initiated to form hydroxyphenoxyl radicals by cleavage of one and/or two OCH_3. Ring-reduction/CO elimination of hydroxyphenoxyl radicals during guaiacol decomposition generated CO, C_2 LHs and C_4 LHs. High yields of C_5 LHs from guaiacol pyrolysis indicated guaiacol could be decomposed as Path 10 and Path 11: CH_3 migration to a neighbor carbon, followed by ring-reduction/CO elimination *via* intermediates (I2 and I3) to produce CO and C_5 LHs. Ring-reduction/CO elimination of hydroxyphenoxyl radicals during syringol decomposition generated CO and C_3 LHs. More C_1 and C_2 fragments were formed from syringol decomposition by loss of two CH_3, followed by the ring rupture, leading to the much higher yields of CH_4 and C_2 LHs. What's more, the increase order of CO yields was not consistent with the oxygen content: lower yield of CO from syringol than from guaiacol. CO_2 yields were much lower than CO yields at all temperatures and RT for all the three model compounds. CO_2 yields increased with oxygen content of phenolic compounds, and the addition of OCH_3 were benefit the formation of CO_2. Path 20 was proposed for the formation of CO_2, which would compete with the formation of CO: CO_2 can be formed through a four-member ring, as, *via* the formation of benzoyl by concerted reaction of OCH_3. The formations of AHs were related with the distribution of C_1–C_5 LHs: more naphthalene from phenol decomposition by the combination of C_5 LHs; more styrene from guaiacol decomposition by the combination of C_2 LHs and/or C_4 LHs; and the addition of OCH_3 benefited the formation of toluene and xylene. PHLs had high yield at temperatures ≤650 °C, and consumed with temperatures increasing to 950 °C. PHLs yields reduced with RT increasing at 750 °C. Phenol and catechol were two main PHLs from guaiacol, while cresols were the main PHLs from syringol in the region of 400 °C–750 °C.

The data produced by this study contribute significantly towards delineating the effects of temperature, RT and OCH_3 on the thermal behaviors of phenolic compounds. Since no kinetic model is currently available for the decomposition of phenol, guaiacol and syringol, the results obtained here will be helpful in the development of a detailed kinetic model for the pyrolysis of phenolic compounds. Since phenol, guaiacol and syringol are typical representatives of solid fuels, and main compounds in volatiles of solid fuels pyrolysis, the present work should be of some use to interpret the mechanisms of vapor-phase reactions during solid fuels pyrolysis. More experimental investigations and numerical simulations on the thermal behaviors of phenolic compounds are expected in future work.

Conflicts of interest

There are no conflicts to declare.

Acknowledgements

This work was supported by Natural Science Foundation of Jiangsu Province (CN) (Grant BK20190156), and the Applied Basic Research Programs of Xuzhou (KC19048).

References

1 L. Dai, Y. Wang, Y. Liu, C. He, R. Ruan, Z. Yu, L. Jiang, Z. Zeng and Q. Wu, A review on selective production of value-added chemicals *via* catalytic pyrolysis of lignocellulosic biomass, *Sci. Total Environ.*, 2020, **749**, 142386, DOI: 10.1016/j.scitotenv.2020.142386.

2 G. S. Ghodake, S. K. Shinde, A. A. Kadam, R. G. Saratale, G. D. Saratale, M. Kumar, R. R. Palem, H. A. AL-Shwaiman, A. M. Elgorban, A. Syed and D. Y. Kim, Review on biomass feedstocks, pyrolysis mechanism and physicochemical properties of biochar: State-of-the-art framework to speed up vision of circular bioeconomy, *J. Cleaner Prod.*, 2021, **297**, 126645, DOI: 10.1016/j.jclepro.2021.126645.

3 C. Liang, X. Wang and Q. Lyu, Experimental investigation on fluidized modification in gasification of preheated coal using oxygen and steam, *Fuel*, 2021, **304**, 121375, DOI: 10.1016/j.fuel.2021.121375.

4 T. Abbasi and S. A. Abbasi, Biomass energy and the environmental impacts associated with its production and utilization, *Renewable Sustainable Energy Rev.*, 2010, **14**, 919–937, DOI: 10.1016/j.rser.2009.11.006.

5 W. H. Chen, W. Farooq, M. Shahbaz, S. R. Naqvi, I. Ali, T. Al-Ansari and N. A. S. Amin, Current status of biohydrogen production from lignocellulosic biomass, technical challenges and commercial potential through pyrolysis process, *Energy*, 2021, **226**, 120433, DOI: 10.1016/j.energy.2021.120433.

6 M. Auersvald, T. Macek, T. Schulzke, M. Staš and P. Šimáček, Influence of biomass type on the composition of bio-oils from ablative fast pyrolysis, *J. Anal. Appl. Pyrolysis*, 2020, **150**, 104838, DOI: 10.1016/j.jaap.2020.104838.

7 H. M. Yang, S. Apparia, S. Kudo, J. Hayash and K. Norinaga, Detailed Chemical Kinetic Modeling of Vapor-Phase Reactions of Volatiles Derived from Fast Pyrolysis of Lignin, *Ind. Eng. Chem. Res.*, 2015, **54**, 6855–6864, DOI: 10.1021/acs.iecr.5b01289.

8 N. Thimthong, S. Appari, R. Tanaka, K. Iwanaga, S. Kudo, J.-i. Hayashi and K. Norinaga, Kinetic modeling of non-catalytic partial oxidation of nascent volatiles derived from fast pyrolysis of woody biomass with detailed chemistry, *Fuel Process. Technol.*, 2015, **134**, 159–167, DOI: 10.1016/j.fuproc.2015.01.029.

9 Z. Xiong, J. Guo, W. Chaiwat, W. Deng, X. Hu, H. Han, Y. Chen, K. Xu, S. Su, S. Hu, Y. Wang and J. Xiang, Assessing the chemical composition of heavy components in bio-oils from the pyrolysis of cellulose, hemicellulose and lignin at slow and fast heating rates, *Fuel Process. Technol.*, 2020, **199**, 106299, DOI: 10.1016/j.fuproc.2019.106299.

10 M. P. Pandey and C. S. Kim, Lignin Depolymerization and Conversion: A Review of Thermochemical Methods, *Chem. Eng. Technol.*, 2011, **34**, 29–41, DOI: 10.1002/ceat.201000270.

11 C. Liu, L. Ye, W. Yuan, Y. Zhang, J. Zou, J. Yang, Y. Wang, F. Qi and Z. Zhou, Investigation on pyrolysis mechanism of guaiacol as lignin model compound at atmospheric pressure, *Fuel*, 2018, **232**, 632–638, DOI: 10.1016/j.fuel.2018.05.162.

12 J. Zakzeski, P. C. Bruijnincx, A. L. Jongerius and B. M. Weckhuysen, The Catalytic Valorization of Lignin for the Production of Renewable Chemicals, *Chem. Rev.*, 2010, **110**, 3552–3599, DOI: 10.1021/cr900354u.

13 L. Zhang, C. Choi, H. Machida and K. Norinaga, Production of light hydrocarbons from organosolv lignin through catalytic hydrogenation and subsequent fast pyrolysis, *J. Anal. Appl. Pyrolysis*, 2021, **156**, 105096, DOI: 10.1016/j.jaap.2021.105096.

14 C. Li, J.-i. Hayashi, Y. F. Sun, L. Zhang, S. Zhang, S. Wang and X. Hu, Impact of heating rates on the evolution of function groups of the biochar from lignin pyrolysis, *J. Anal. Appl. Pyrolysis*, 2021, **155**, 105031, DOI: 10.1016/j.jaap.2021.105031.

15 J. Yu, D. Wang and L. Sun, The pyrolysis of lignin: Pathway and interaction studies, *Fuel*, 2021, **290**, 120078, DOI: 10.1016/j.fuel.2020.120078.

16 Q. Lu, W. Xie, B. Hu, J. Liu, W. Zhao, B. Zhang and T.-p. Wang, A novel interaction mechanism in lignin pyrolysis: Phenolics-assisted hydrogen transfer for the decomposition of the β-O-4 linkage, *Combust. Flame*, 2021, **225**, 395–405, DOI: 10.1016/j.combustflame.2020.11.011.

17 J. Huang and C. He, Pyrolysis mechanism of α-O-4 linkage lignin dimer: A theoretical study, *J. Anal. Appl. Pyrolysis*, 2015, **113**, 655–664, DOI: 10.1016/j.jaap.2015.04.012.

18 M. Akazawa, Y. Kojima and Y. Kato, Effect of pyrolysis temperature on the pyrolytic degradation mechanism of β-aryl ether linkages, *J. Anal. Appl. Pyrolysis*, 2016, **118**, 164–174, DOI: 10.1016/j.jaap.2016.02.001.

19 J. Huang, C. He, C. Liu, H. Tong, L. Wu and S. Wu, A computational study on thermal decomposition mechanism of β-1 linkage lignin dimer, *Comput. Theor. Chem.*, 2015, **1054**, 80–87, DOI: 10.1016/j.comptc.2014.12.007.

20 M. Nowakowska, O. Herbinet, A. Dufour and P. A. Glaude, Detailed kinetic study of anisole pyrolysis and oxidation to understand tar formation during biomass combustion and gasification, *Combust. Flame*, 2014, **161**, 1474–1488, DOI: 10.1016/j.combustflame.2013.11.024.

21 A. M. Scheer, C. Mukarakate, D. J. Robichaud, M. R. Nimlos, H. H. Carstensen and G. B. Ellison, Unimolecular thermal decomposition of phenol and d(5)-phenol: Direct observation of cyclopentadiene formation *via* cyclohexadienone, *J. Chem. Phys. A*, 2012, **136**, 044309, DOI: 10.1063/1.3675902.

22 Z. F. Xu and M. C. Lin, Ab initio kinetics for the unimolecular reaction C6H5OH -> CO+C5H6, *J. Phys. Chem. A*, 2006, **110**, 1672–1677, DOI: 10.1021/jp055241d.

23 M. Altarawneh, B. Z. Dlugogorski, E. M. Kennedy and J. C. Mackie, Theoretical Study of Unimolecular Decomposition of Catechol, *J. Phys. Chem. A*, 2010, **114**, 1060–1067, DOI: 10.1021/jp909025s.

24 E. B. Ledesma, N. D. Marsh, A. K. Sandrowitz and M. J. Wornat, An experimental study on the thermal decomposition of catechol, *Proc. Combust. Inst.*, 2002, **29**, 2299–2306, DOI: 10.1016/S1540-7489(02)80280-2.

25 H. M. Yang, Y. Furutani, S. Kudo, J. Hayash and K. Norinaga, Experimental investigation of thermal decomposition of dihydroxybenzene isomers: catechol, hydroquinone, and resorcinol, *J. Anal. Appl. Pyrolysis*, 2016, **120**, 321–329, DOI: 10.1016/j.jaap.2016.05.019.

26 L. Khachatryan, R. Asatryan, C. McFerrin, J. Adounkpe and B. Dellinger, Radicals from the Gas-Phase Pyrolysis of Catechol. 2. Comparison of the Pyrolysis of Catechol and Hydroquinone, *J. Phys. Chem. A*, 2010, **114**, 10110–10116, DOI: 10.1021/jp1054588.

27 A. V. Friderichsen, E. J. Shin, R. J. Evans, M. R. Nimlos, D. C. Dayton and G. B. Ellison, The pyrolysis of anisole (C6H5OCH3) using a hyperthermal nozzle, *Fuel*, 2001, **80**, 1747–1755, DOI: 10.1016/S0016-2361(01)00059-X.

28 A. M. Scheer, C. Mukarakate, D. J. Robichaud, G. B. Ellison and M. R. Nimlos, Radical Chemistry in the Thermal Decomposition of Anisole and Deuterated Anisoles: An Investigation of Aromatic Growth, *J. Phys. Chem. A*, 2010, **114**, 9043–9056, DOI: 10.1021/jp102046p.

29 J. C. Mackie, K. R. Doolan and P. F. Nelson, Kinetics of the Thermal Decomposition of Methoxybenzene (Anisole), *Cheminform*, 1989, **20**, 664–670, DOI: 10.1021/j100339a033.

30 A. M. Scheer, C. Mukarakate, D. J. Robichaud, M. R. Nimlos and G. B. Ellison, Thermal Decomposition Mechanisms of the Methoxyphenols: Formation of Phenol, Cyclopentadienone, Vinylacetylene, and Acetylene, *J. Phys. Chem. A*, 2011, **115**, 13381–13389, DOI: 10.1021/jp2068073.

31 T. T. P. Nguyen, T. V.-T. Mai and L. K. Huynh, Detailed kinetic modeling of thermal decomposition of guaiacol - A model compound for biomass lignin, *Biomass Bioenergy*, 2018, **112**, 45–60, DOI: 10.1016/j.biombioe.2018.02.006.

32 M. M. Suryan, S. A. Kafafi and S. E. Stein, The Thermal Decomposition of Hydroxy- and Methoxy- Substituted Anisoles, *J. Am. Chem. Soc.*, 1989, **111**, 1423–1429, DOI: 10.1021/ja00186a042.

33 C. Liu, Y. Y. Zhang and X. L. Huang, Study of guaiacol pyrolysis mechanism based on density function theory, *Fuel Process. Technol.*, 2014, **123**, 159–165, DOI: 10.1016/j.fuproc.2014.01.002.

34 M. Asmadi, H. Kawamoto and S. Saka, Thermal reactions of guaiacol and syringol as lignin model aromatic nuclei, *J. Anal. Appl. Pyrolysis*, 2011, **92**, 88–98, DOI: 10.1016/j.jaap.2011.04.011.

35 J. B. Huang, C. Liu, L. R. Ren, H. Tong, W. M. Li and D. Wu, Studies on pyrolysis mechanism of syringol as lignin model compound by quantum chemistry, *J. Fuel Chem. Technol.*, 2013, **41**, 657–666, DOI: 10.1016/S1872-5813(13)60031-6.

36 A. E. Harman-Ware, M. Crocker, A. P. Kaur, M. S. Meier, D. Kato and B. Lynn, Pyrolysis–GC/MS of sinapyl and

coniferyl alcohol, *J. Anal. Appl. Pyrolysis*, 2013, **99**, 161–169, DOI: 10.1016/j.jaap.2012.10.001.

37 E. B. Ledesma, J. N. Hoang, Q. Nguyen, V. Hernandez, M. P. Nguyen, S. Batamo and C. K. Fortune, Unimolecular Decomposition Pathway for the Vapor-Phase Cracking of Eugenol, A Biomass Tar Compound, Energ, *Fuel*, 2013, **27**, 6839–6846, DOI: 10.1021/ef401760c.

38 E. J. Shin, M. R. Nimlos and R. J. Evans, A study of the mechanisms of vanillin pyrolysis by mass spectrometry and multivariate analysis, *Fuel*, 2001, **80**, 1689–1696, DOI: 10.1016/S0016-2361(01)00055-2.

39 G. Z. Jiang, D. J. Nowakowski and A. V. Bridgwater, Effect of the Temperature on the Composition of Lignin Pyrolysis Products, *Energy Fuels*, 2010, **24**, 4470–4475, DOI: 10.1021/ef100363c.

40 K. Norinaga, H. M. Yang, R. Tanaka, S. Apparia, K. Iwanaga, Y. Takashima, S. Kudo, T. Shoji and J.-i. Hayash, A mechanistic study on the reaction pathways leading to benzene and naphthalene in cellulose vapor phase cracking, *Biomass Bioenergy*, 2014, **69**, 144–154, DOI: 10.1016/j.biombioe.2014.07.008.

41 K. Moshammer, L. Seidel, Y. Wang, H. Selim, S. M. Sarathy, F. Mauss and N. Hansen, Aromatic ring formation in opposed-flow diffusive 1,3-butadiene flames, *Proc. Combust. Inst.*, 2017, **36**, 947–955, DOI: 10.1016/j.proci.2016.09.010.

42 N. B. Poddar, S. Thomas and M. J. Wornat, Polycyclic aromatic hydrocarbons from the co-pyrolysis of 1,3-butadiene and propyne, *Proc. Combust. Inst.*, 2013, **34**, 1775–1783, DOI: 10.1016/j.proci.2012.05.013.

43 Y. Matsukawa, K. Ono, K. Dewa, A. Watanabe, Y. Saito, Y. Matsushita, H. Aoki, K. Era, T. Aoki and T. Yamaguchi, Reaction pathway for nascent soot in ethylene pyrolysis, *Combust. Flame*, 2016, **167**, 248–258, DOI: 10.1016/j.combustflame.2016.02.008.

44 J. Filley and J. T. McKinnon, Dimerization of cyclopentadienyl radical to produce naphthalene, *Combust. Flame*, 2001, **124**, 721–723, DOI: 10.1016/S0010-2180(00)00223-6.

45 V. Chernov, M. J. Thomson, S. B. Dworkin, N. A. Slavinskaya and U. Riedel, Soot formation with C_1 and C_2 fuels using an improved chemical mechanism for PAH growth, *Combust. Flame*, 2014, **161**, 592–601, DOI: 10.1016/j.combustflame.2013.09.017.

46 Y. Furutani, S. Kudo, J. Hayashi and K. Norinaga, Theoretical Study on Reaction Pathways Leading to CO and CO_2 in the Pyrolysis of Resorcinol, *J. Phys. Chem. A*, 2017, **121**, 631–637, DOI: 10.1021/acs.jpca.6b05168.

47 V. B. F. Custodis, P. Hemberger, Z. Q. Ma and J. A. Bokhoven, Mechanism of Fast Pyrolysis of Lignin: Studying Model Compounds, *J. Phys. Chem. B*, 2014, **118**, 8524–8531, DOI: 10.1021/jp5036579.